Available online at www.sciencedirect.com
SCIENCE DIRECT®
Journal of Sound and Vibration 286 (2005) 81–96
JOURNAL OF SOUND AND VIBRATION
www.elsevier.com/locate/jsvi

A wave model for rigid-frame porous materials using lumped parameter concepts

S. Rossetti, P. Gardonio*, M.J. Brennan

Institute of Sound and Vibration Research, University of Southampton, Highfield, Southampton SO17 1BJ, UK

Received 19 January 2004; received in revised form 29 April 2004; accepted 28 September 2004
Available online 1 January 2005

Abstract

The work presented in this paper concerns the behaviour of porous media when exposed to a normal incidence sound field. A propagating wave model based on lumped parameter concepts of acoustic mass, stiffness and damping is used to investigate the absorption phenomena due to the wave propagation in the layer(s) and interference effects due to the wave reflection–transmission at the interfaces of the layer(s). Results from the theoretical model have been validated by measurements on samples of consolidated rubber granulate material. Two typical installations where a layer of porous material is placed next to a rigid wall, and where it is placed at a distance from a rigid wall are used as reference cases. The geometrical and physical properties of porous materials can be described by such parameters as the non-dimensional shape factor and the porosity. The propagating model introduced is used to investigate the effect of these two parameters on acoustic absorption and thus relate the physical properties to the acoustic behaviour.

PACS: 43.55.Ev

1. Introduction

In this paper the acoustic behaviour of rigid-frame porous materials is discussed. This area has been investigated by several researchers [1–4], but one of the most significant contributions is by

*Corresponding author. Tel.: +44 23 8059 4933; fax: +44 238 059 3190.
E-mail address: pg@isvr.soton.ac.uk (P. Gardonio).

0022-460X/$ - see front matter
doi:10.1016/j.jsv.2004.09.034

Johnson et al. [2]. In their work they established high- and low-frequency limits for the dynamic tortuosity and permeability and introduced a parameter to describe the characteristics of connected pores. Their expressions for tortuosity and permeability are widely used in models for rigid-frame porous materials. The thermal effects in such materials have been discussed by Lafarge et al. [3] using a similar approach to that in Ref. [2].

The theory in this field is quite complex as it involves acoustics, dynamics of fluids and statistics; thus simplification is necessary in order to improve the physical understanding of the absorption mechanisms and in such a way as to simplify the design procedures of sound insulation with porous material linings. Brennan and To [5] described rigid-frame porous materials in terms of acoustic mass, stiffness and damping lumped parameters. These concepts are further developed in this paper by introducing the non-dimensional shape factor M and the porosity, h, effects. Also, a propagating wave model based on lumped parameter concepts is used so that the absorption phenomena due to the wave propagation in the layer(s) and interference effects due to the wave reflection–transmission at the interfaces of the layer(s) are separately discussed and analysed. Absorption and reflection coefficients are derived with reference to a plane acoustic wave, which is incident normal to the surface of the porous layer, but this analysis could be applied also to plane waves that are incident to the surface of the layer at an angle provided the porous material is locally reacting.

The model is validated by measurements of acoustic absorption on samples of consolidated rubber granulated material produced at the University of Bradford, for which data of flow resistivity, tortuosity and porosity were available [6].

Two typical installations are studied using the model, one where a layer of porous material is placed next to a rigid wall, and the other where the porous material is placed at a distance from a rigid wall.

2. Acoustic waves in porous materials

In this section, the theoretical background of sound propagation in rigid-frame porous material is reviewed. For plane wave sound propagation in gases contained within rigid-frame porous materials the wave equation is given by [7]

$$\frac{\partial^2 p}{\partial x^2} - \left(\frac{s\rho_0}{\kappa}\right)\frac{\partial^2 p}{\partial t^2} - \left(\frac{\sigma h}{\kappa}\right)\frac{\partial p}{\partial t} = 0, \tag{1}$$

where p is pressure and t is time, κ is the effective bulk modulus of the gas, ρ_0 the density of air, h the porosity of the material, σ is the flow resistivity and s is the structure factor. Assuming a solution with time and space dependence of the form $e^{j(\omega t - k_c x)}$, the complex impedance, Z_c, and the complex wavenumber, k_c, in a pore are given by [1]

$$Z_c = (\rho_e \kappa)^{1/2}, \quad k_c = \omega\left(\frac{\rho_e}{\kappa}\right)^{1/2}, \tag{2,3}$$

where ω is the circular frequency. To describe the harmonic response of a locally reacting rigid-frame porous material, knowledge of these two parameters is sufficient.

2.1. Effective density and bulk modulus

Most models of rigid-frame porous materials are based on the work by Johnson et al. [2] and Lafarge et al. [3]. Expressions for the complex density and the bulk modulus are, respectively, given by

$$\rho_e = \rho_0 \alpha_\infty \left(1 + \mathrm{j}\,\frac{\eta h}{\rho_0 \alpha_\infty k_0 \omega}\left(1 - \mathrm{j}\,\frac{4\rho_0 \alpha_\infty^2 k_0^2 \omega}{\eta h^2 \Lambda^2}\right)^{1/2}\right), \tag{4}$$

$$\kappa = \frac{\gamma P}{\gamma - (\gamma - 1)\left(1 + \mathrm{j}\,\frac{\eta h}{\rho_0 Pr\, k_0' \omega}\left(1 - \mathrm{j}\,\frac{4\rho_0 Pr k_0'^2 \omega}{\eta h^2 \Lambda'^2}\right)^{1/2}\right)^{-1}}, \tag{5}$$

where P is the static pressure α_∞ is the tortuosity, k_0 is the viscous permeability, k_0' is the thermal permeability, η is the viscosity, γ is the ratio of the specific heats, Pr is the Prandtl number, Λ is the characteristic viscous dimension and Λ' is the characteristic thermal dimension.

The network of pores in a rigid-frame porous material can be seen as a system of small necks and volumes. Therefore equivalent acoustic mass, damping and stiffness effects for the whole material can be derived. If the real and imaginary parts in Eqs. (4) and (5) are isolated then it is possible to identify the effects of density and bulk modulus in terms of mass, stiffness and damping whose impedances are given by [8]

$$Z_m = \mathrm{j}\omega m, \quad Z_k = -\mathrm{j}\,\frac{k}{\omega}, \quad Z_c = c, \tag{6a–c}$$

where m, k, c are the equivalent acoustic mass, stiffness and damping for the porous layer, respectively. The frequency responses of these equivalent acoustic impedances are visualized in Fig. 1(a) which shows that the mass effect rises proportionally with frequency while the stiffness effect decays proportionally with frequency and the damping effect is constant throughout. As shown in Fig. 1(b), the impedances of the equivalent acoustic mass and stiffness are complex with phase $\pm 90^\circ$, respectively, while the impedance of equivalent damping is positive-real.

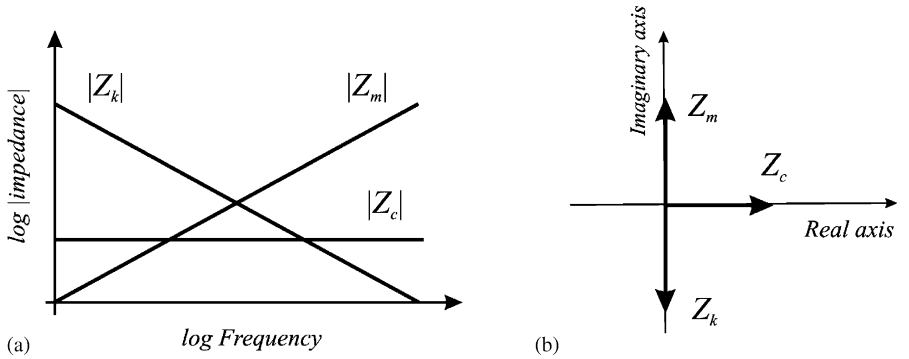

Fig. 1. Equivalent mass, stiffness and damping impedances.

Following the formulation presented by Brennan and To [5] the normalized effective density can be expressed as follows:

$$\frac{\rho_e}{\rho_0\alpha_\infty} = 1 + \left\{\frac{(1+(\Omega M/2)^2)^{1/2}-1}{2\Omega^2}\right\}^{1/2} - \mathrm{j}\left\{\frac{(1+(\Omega M/2)^2)^{1/2}+1}{2\Omega^2}\right\}^{1/2}, \tag{7}$$

where $\Omega = \omega/\omega_t$, with $\omega_t = h\eta/k_0\rho_0\alpha_\infty$, and the non-dimensional shape factor $M = 8\alpha_\infty k_0/h\Lambda^2$ which depends on the microstructure of the material. The equivalent acoustic mass impedance given in Eq. 6(a) can be expressed in terms of the real and imaginary components of the complex density given in Eq. (7) with a positive real part and a negative imaginary part. The top plot in Fig. 2 shows that the real part of the complex density is almost constant for the whole frequency range while the bottom plot in Fig. 2 indicates that the imaginary part varies as $1/\omega$ at low frequencies such that $\Omega<1$. Therefore, the equivalent acoustic mass contribution in a porous material is proportional to the real part of the complex density whereas the imaginary part of the complex density provides the equivalent acoustic damping effect due to the interaction between the rigid frame of the material and the fluid contained in the pores. At low frequencies, when $\Omega<1$, the damping-like behaviour (imaginary part) dominates over the mass like behaviour (real part) whereas at higher frequencies, such as $\Omega>1$, it is the mass which dominates over the damping, and ω_t is the transition frequency from the damping to the mass-like behaviour for the reference case where $M = 0$.

Different authors have suggested different values for M according to the specific structure of the material, for example $M = 1$ for cylindrical slits [2], $M = 5$ or 6 for two granular materials [9,10]. According to the top plot in Fig. 2, the mass effect significantly varies with M at low frequencies, but this is not significant, since when $\Omega<1$ the damping (which is not affected by variation of M) dominates over the mass-like behaviour. In contrast, at higher frequencies when $\Omega>1$ it is the damping effect that appreciably varies with M but in this case the mass effect (which is not affected by variation of M) dominates over the damping effect.

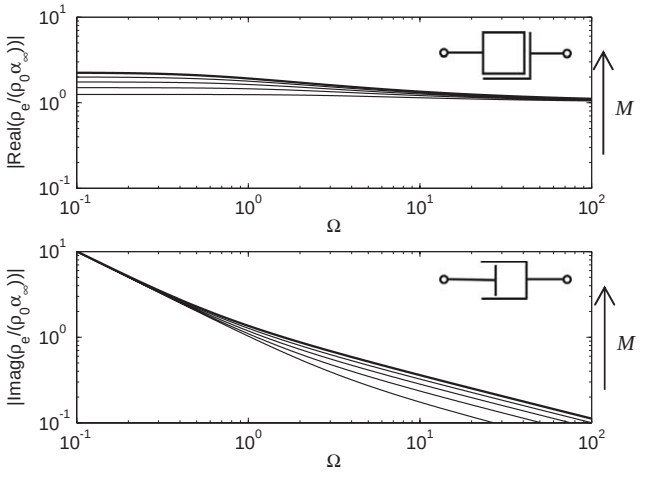

Fig. 2. Absolute values of the real and imaginary parts of the normalized effective density with reference to increasing values of the non-dimensional shape factor M (1–5). The arrows indicate rising values of M and the thick line corresponds to $M = 5$.

Similar to the effective density, the bulk modulus given in Eq. (5) can also be expressed in terms of real and imaginary parts to give:

$$\frac{\kappa}{\gamma P} = \frac{\bar{\Omega}^2 + \gamma}{\bar{\Omega}^2 + \gamma^2} + \mathrm{j}\,\frac{\bar{\Omega}(\gamma - 1)}{\bar{\Omega}^2 + \gamma^2}, \tag{8}$$

where a term $\bar{\Omega}M'/2$ has been neglected in the derivation [5]. This expression includes a thermal dimensionless coefficient $M' = 8k'_0/h\Lambda'^2$, where k'_0 is the thermal permeability and Λ' is the characteristic thermal dimension. Also in this case the frequency is written in non-dimensional form $\bar{\Omega} = \omega/\bar{\omega}_t$, where $\bar{\omega}_t = \omega_t(M/A')$ with $A' = 8\,Pr\,k'_0/h\Lambda^2$.

The equivalent acoustic stiffness k given in Eq. 6(b) can be expressed in terms of the real and imaginary components of the complex bulk modulus given in Eq. (8). The top plot in Fig. 3 shows that the real part is nearly constant for the whole frequency range while the bottom plot indicates that the imaginary part varies in proportion with ω at low frequencies such that $\Omega < 1$. Thus, the equivalent acoustic stiffness effect in a porous material is due to the real part of the complex bulk modulus whereas the imaginary part provides the losses. Brennan and To [5] have analytically compared the viscous and thermal damping effects for a material that has similar pore sizes throughout its volume. They found that even at the frequency when the loss factor is maximum, the viscous damping is much greater than the thermal losses, which can thus be neglected. However Henry et al. [11] have shown that this approximation is not valid for very thin layers directly in contact with an impervious rigid backing. Also, as shown in the top plot of Fig. 3, the reactive stiffness term is approximately 0.85 over the whole frequency range.

In conclusion a rigid-frame porous material can be described by a complex density and a complex bulk modulus which represent, respectively, equivalent acoustic mass–viscous damping behaviour and equivalent acoustic stiffness–hysteretic damping behaviour.

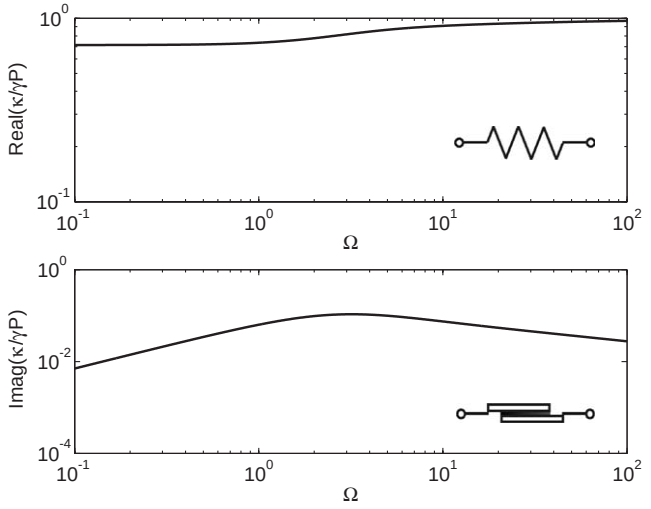

Fig. 3. Absolute values of the real and imaginary parts of the effective bulk modulus.

2.2. Acoustic wavenumber and impedance

Once the complex density and bulk modulus have been determined, the wavenumber and the impedance can be calculated. However these are rather complicated expressions that could be simplified by assuming that the thermal losses can be neglected; also the bulk modulus can be considered to be constant with frequency and given by $\kappa = P$. This will have a small effect on the predicted wavenumber and impedance at high frequencies [5]. The expressions for the impedance and wavenumber, normalized to the corresponding value in air, thus become

$$\hat{Z}_c = \frac{1}{h}\left(\frac{\alpha_\infty}{\gamma}\right)^{1/2}\left(\frac{\rho_e}{\rho_a}\right)^{1/2}, \quad \hat{k}_c = (\alpha_\infty\gamma)^{1/2}\left(\frac{\rho_e}{\rho_a}\right)^{1/2}. \tag{9,10}$$

Eq. (9) represents the average characteristic impedance of a porous medium and thus includes the corresponding porosity (ratio of the cross-sectional area of one channel and the surface area per channel). Although these are relatively simple mathematical expressions, they do not provide a direct physical interpretation of the reflection of incident waves to the porous material (acoustic impedance) and propagation/dissipation (acoustic wavenumber) of acoustic waves in the porous material. However, as discussed in Section 2.1 they can be reformulated in terms of equivalent acoustic mass, stiffness and damping concepts by isolating the real and imaginary parts. The plot in Fig. 4a shows that the real and imaginary parts of the characteristic acoustic impedance normalised with reference to the value in air Z_0 are respectively positive and negative. At low frequencies where $\Omega<1$, the amplitude of the real part varies with frequency as $1/\sqrt{\omega}$ and indicates a dissipative behaviour. For higher frequencies, when $\Omega>1$, the real part converges to a constant value which indicates a typical viscous damping behaviour and the amplitude of the imaginary part varies with frequency as $1/\omega$ and thus it indicates an equivalent acoustic stiffness behaviour.

The propagation and dissipation of sound in a porous material is determined by the acoustic wavenumber. These phenomena can be illustrated by considering the real and imaginary parts of the acoustic wavenumber normalised with reference to the value in air k_0 which are shown in Fig. 4b. At low frequencies when $\Omega<1$, the amplitude of the real part varies with frequency as

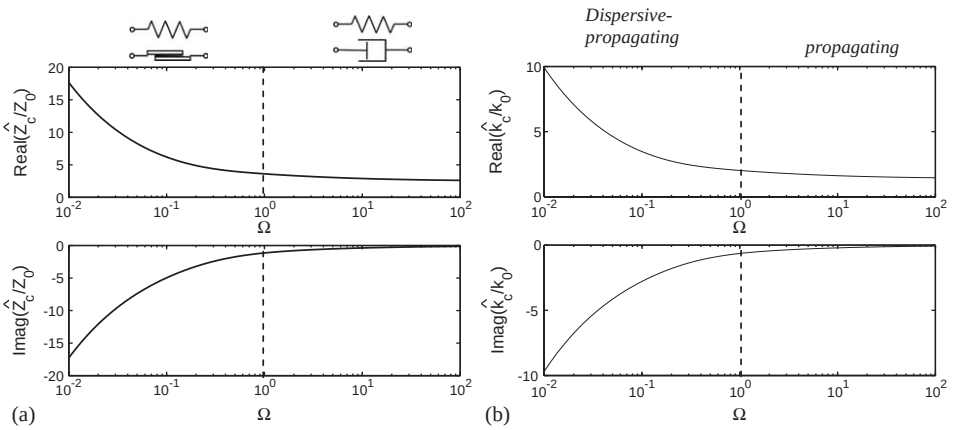

Fig. 4. Real and imaginary parts of the normalized acoustic impedance (a) and acoustic wavenumber (b).

$1/\sqrt{\omega}$ which indicates a dispersive propagation phenomena [12]. In contrast, at higher frequencies, when $\Omega > 1$, the real part becomes constant which indicates non-dispersive wave propagation and the amplitude of the imaginary part varies with frequency as $1/\omega$ which indicates a typical hysteretic loss behaviour [12].

3. Reflection, transmission of sound in finite layers of porous materials

A simple representation of a propagating time harmonic wave in a generic medium 1 (fluid) which impinges on a semi-infinite medium 2 (porous material) is shown in Fig. 5 where ρ_1 and c_1 are, respectively, the density and speed of sound in the fluid on the left-hand side and ρ_2 and c_2 are, respectively, the density and speed of sound in the porous material on the right-hand side. The wave impinging on medium 2 (incident wave) is partly absorbed/dissipated inside the medium itself, and partly reflected. For this system the *reflection* and *transmission* coefficients can be specified as follows: the *interface reflection coefficient* is defined as the ratio between the reflected and the incident sound pressure and the *interface transmission coefficient* is equal to the ratio of the transmitted and the incident sound pressure:

$$r = \frac{p_r}{p_i} = \frac{P_r}{P_i}, \quad t = \frac{p_t}{p_i} = \frac{P_t}{P_i}, \tag{11,12}$$

where $p_i = P_i e^{j(\omega t - k_1 x)}$, $p_r = P_r e^{j(\omega t + k_1 x)}$, $p_t = P_t e^{j(\omega t - k_2 x)}$ are the sound pressure of the incident, reflected and transmitted waves and P_i, P_r, P_t are the relative complex amplitudes (phasors) for $t = 0$ and $x = 0$ at the interface. By taking into account the continuity of pressure and of the normal component of the particle velocity at the interface between the two media [8], it is possible to derive expressions for both r and t:

$$r = \frac{z_2 - z_1}{z_2 + z_1}, \quad t = \frac{2z_2}{z_2 + z_1}, \tag{13,14}$$

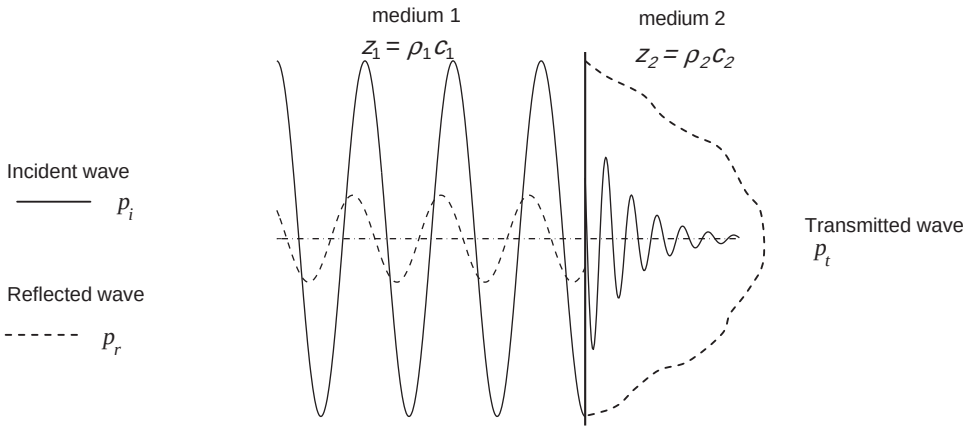

Fig. 5. Incident, transmitted and reflected waves in a simple case of waves impinging a semi-infinite porous material.

where $z_1 = \rho_1 c_1$ and $z_2 = \rho_2 c_2$ are the characteristic impedances of the two media. Fig. 5 illustrates wave reflection and propagation in a semi-infinite porous medium where the incident harmonic wave (solid line) is partially reflected (dashed line) and partially transmitted within the layer where it decays because of the damping effects of the porous material. Note that there is a phase shift for the reflected and transmitted waves at the interface between the fluid and porous material, which is due to the complex part of the characteristic impedance.

In the case of a finite thickness layer of porous material the global reflection and transmission coefficients can also be defined. Fig. 6 shows the wave propagation paths for a general case of an incident plane acoustic wave to a layer of porous material of finite thickness. In this case the incident wave transmitted into the layer will generate standing waves due to the interference of the positive and negative going acoustic waves in the layer [13]. These two propagating components will give rise, respectively, to indirect reflections of sound into the first medium and to transmission of sound into the third medium as shown in the schematic of Fig. 6. The reflection of the incident wave in layer one is therefore given by two components: first the direct reflection of the incident wave at the interface between the first medium and the layer of porous material and second the indirect reflection due to the negative components of the propagating waves within the layer that will transmit back into the first medium an acoustic wave each time they impinge on the left-hand side interface of the porous layer of thickness d_1. As a result the global reflection coefficient is given by [14]

$$R_L = r_{12} + \frac{t_{12}t_{21}r_{23}\mathrm{e}^{-\mathrm{j}k_2 2d_1}}{1 - \{r_{21}r_{23}\mathrm{e}^{-\mathrm{j}k_2 2d_1}\}} \tag{15}$$

(if the porous material is rigidly backed, then $r_{23} = 1$).

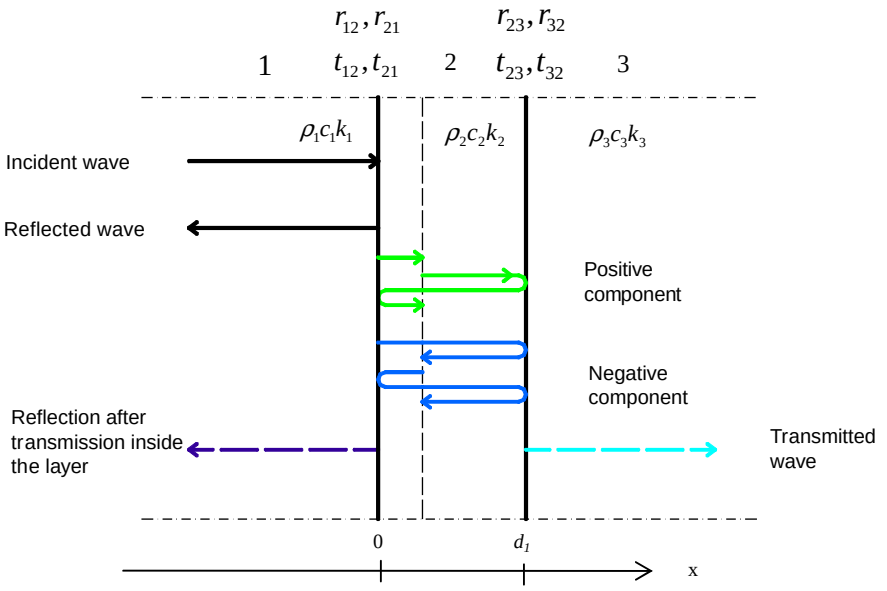

Fig. 6. Schematic showing the patterns of the incident, reflected and transmitted waves for a generic layer of porous material.

Similarly the sound transmission into the third medium is given by the positive components of the propagating waves within the layer that will transmit into the third medium an acoustic wave each time they impinge on the right-hand side interface of the porous layer. Thus the global transmission coefficient T is found to be [14]:

$$T = \frac{t_{12}t_{23}\mathrm{e}^{-\mathrm{j}k_2 d_1}}{1 - r_{21}r_{23}\mathrm{e}^{-\mathrm{j}k_2 2d_1}}. \tag{16}$$

If, as shown in Fig. 7, a rigid backing is placed at a distance from the right-hand side of the porous layer in such a way as to leave an air gap, then standing waves are generated in both the layer of porous material and the air gap. Following the same mechanisms described above, these standing waves will produce series of forward and backward sound transmissions effects between the layer of porous material and the air gap and this will result into an overall indirect reflection of sound into the first medium such that, as described in Ref. [14], the total reflection coefficient is

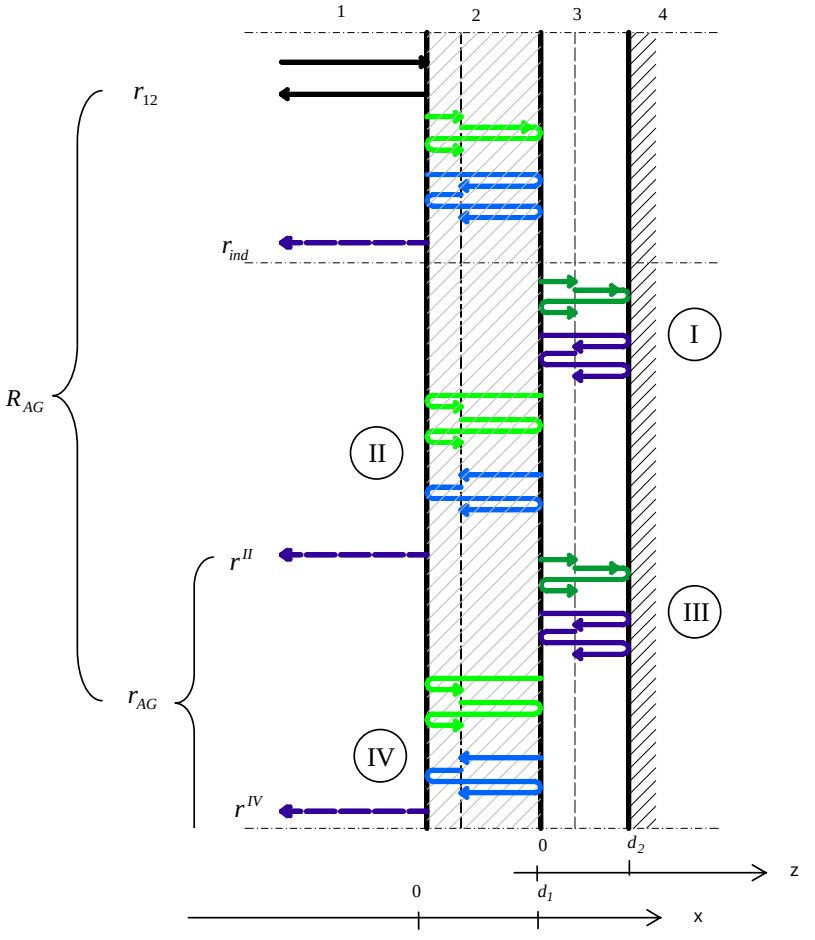

Fig. 7. Schematic of a layer of porous material of thickness d_1 placed at a distance d_2 from a rigid wall.

given by

$$R_{AG} = R_L + r_{AG}, \tag{17}$$

where

$$r_{AG} = \frac{t_1 e^{-j2(k_2 d_1 + k_3 d_2)}}{(1 - r_1 e^{-jk_2 2d_1})^2 (1 - r_2 e^{-jk_3 2d_2}) - (1 - r_1 e^{-jk_2 2d_1}) \cdot t_2 e^{-j2(k_2 d_1 + k_3 d_2)}} \tag{18}$$

and $t_1 = t_{12}t_{21}t_{23}t_{32}r_{34}$, $t_2 = t_{23}t_{32}r_{21}r_{34}$, $r_1 = r_{21}r_{23}$ and $r_2 = r_{32}r_{34}$, and d_2 is the cavity depth. The combination of the wave models for the three cases considered in this paper, semi-infinite, rigidly backed and rigidly backed with an air gap, together with the simplified expressions for the characteristic acoustic impedance and wavenumber given in Section 2, provides a direct interpretation of the physical phenomena that control the absorption properties of rigid-frame porous materials.

In order to validate the wave model and the simplified representation of the complex impedance and wavenumber presented in this paper, measurements of acoustic absorption coefficient with an impedance tube have been taken on three samples of consolidated rubber granulate materials with different physical and geometrical properties, which are given in Table 1, produced at the University of Bradford [6]. The absorption coefficient is the quantity that describes their acoustic absorption properties and it is derived from the reflection coefficient by means of equation [8]:

$$A = 1 - |R|^2, \tag{19}$$

where R is the reflection coefficient of the layer. Measurements of normal incidence absorption coefficients have been performed using the technique developed in Ref. [15]. The wave model has then been used to compare theoretical results with the experimental absorption coefficients measured for the three samples. Data of porosity, tortuosity and flow resistivity were available for the samples, characterized by different grain sizes as summarized in Table 1. Figs. 8a–c show theoretical and experimental curves of absorption coefficients for the three samples (J, K and L) under rigid backing conditions. In general the theoretical predictions agree quite well with the experimental results. In Fig. 8d the absorption coefficient concerning sample L with a 26 mm air gap is given which also indicates good agreement between theoretical and measured absorption. There has been considerable discussion about the suitable value of non-dimensional shape factor M (see Refs. [2,9,10]), and specific values have been proposed for different pore shapes in porous media. In the present study a procedure of least squares fit of the theoretical plots and experimental data has been adopted so that $M_J = 6$, $M_K = 3.5$ and $M_L = 3$.

Table 1
Non-acoustic properties for three samples of consolidated rubber granulate material (measured at the University of Bradford)

Sample	Grain size (mm)	Porosity (%)	Tortuosity α_∞	Flow resistivity R (N s m^{-4})	Thickness (mm)
J	1.4–2	36.0	1.63	1.98×10^4	20
K	1–1.4	35.5	1.64	5.15×10^4	20
L	0.71–1	36.4	1.61	9.22×10^4	20

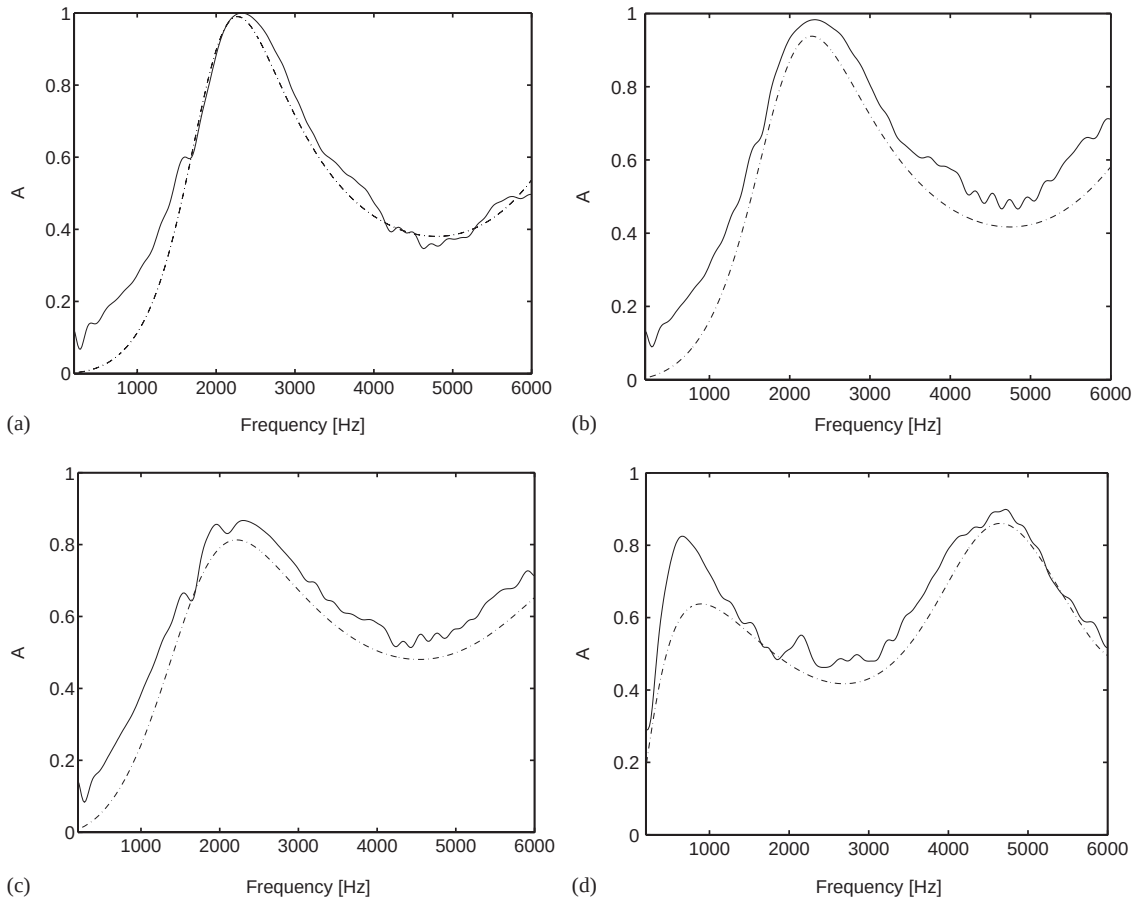

Fig. 8. Plots of theoretical (dashed line) and experimental (solid line) curves for the absorption coefficient: (a) sample J, (b) sample K, (c) sample L, (d) sample L with 26 mm air gap. The tuned frequency ω_t is 3644, 9290 and 17,371 rad/s for the three samples, respectively.

4. Non-dimensional shape factors and porosity effects

In the following subsections the wave model presented in Section 3 and the simplified expressions for the complex impedance and wavenumber given in Section 2 are used to briefly introduce the absorption characteristics of porous media in two practical application cases, where a layer of porous material is placed next to a rigid wall or placed at a distance from it.

Following the effects of non-dimensional shape factors and porosity are investigated. The analysis is carried out with reference to values for the tortuosity, porosity and other non-acoustical parameters used in Ref. [6] and here summarized in Table 2, which correspond to measured values for random packing of beads.

The dash–dotted line in Fig. 9 represents the absorption coefficient for the semi-infinite case. The impinging sound energy is absorbed according to the physical and geometrical properties of the material itself; however, in general the acoustic absorption is small in the low-frequency region

where the porous layer reacts as an equivalent acoustic spring and approximately settles on a fixed value in the high-frequency region, which is controlled by the equivalent acoustic damping effect. When the material is characterized instead by a finite thickness the shape of the curve is characterized by an oscillating pattern that becomes more and more pronounced as the thickness of the layer becomes smaller. This oscillating phenomena could be explained by considering the wave propagation model described in Fig. 6. In this case, the reflection of sound is determined by the *direct reflection* at the interface plus a series of "delayed" *indirect reflections* that comes from the acoustic waves propagating within the layer. The amplitudes and phases of these delayed indirect reflections depend upon three phenomena: first, the transmissions coefficients at the left-hand interface; second, the reflections at the left- and right-hand interfaces which, for relatively thin layers, determine the generation of standing waves and third, the dissipation of the propagating waves within the layer. Considering a given damping effect in the porous material, for relatively thick layers even the first indirect reflection is negligible since the energy of the first

Table 2
Data for the non-acoustical parameters used in the model [9]

Parameter	Value
Porosity h	0.4
Viscous permeability k_0	1.5e−9 m^2
Tortuosity α_∞	1.37
Density ρ_0 at 20 °C	1.2 $kg\,m^{-3}$
Dynamic viscosity η at 20 °C	18.22e−6 $N\,s\,m^{-2}$
Ratio of specific heats γ	1.4

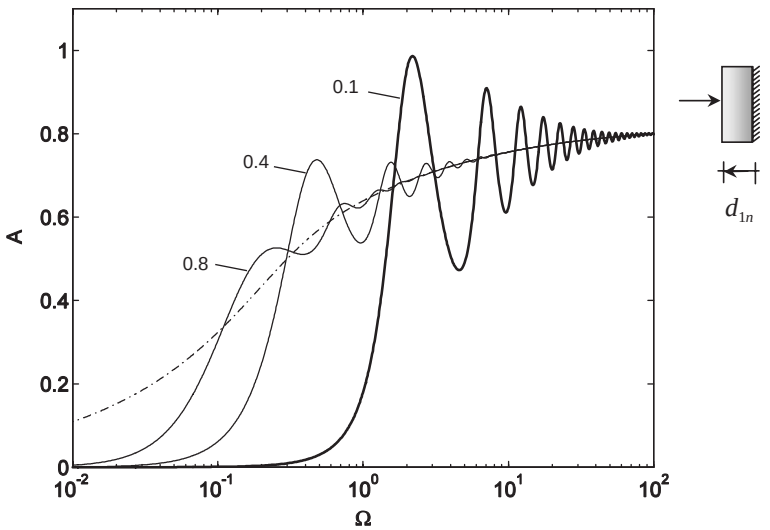

Fig. 9. Absorption coefficient curves corresponding to three different values of the layer thickness (solid lines) and reference curve for a semi-infinite porous material (dash–dotted line). All the curves are plotted for a value of $M = 5$. $d_{1n} = 0.1, 0.4, 0.8$.

transmitted wave to the layer is dissipated within the layer itself before it reflects back to the left-hand side interface. However, as the thickness of the layer becomes smaller the dissipation of the first indirect reflection is reduced. Moreover there are some frequencies where standing waves are generated within the layer so that there could be several indirect reflections that constructively contribute to form the reflected wave. These indirectly reflected waves will have varying phase that at some frequencies will destructively interfere with the directly reflected wave and at other frequencies will instead constructively interfere with the directly reflected wave. As a result, the absorption coefficient is characterized by an oscillatory curve that, as shown in Fig. 9, becomes more uneven as the thickness gets smaller. The curve with the widest oscillations in Fig. 9 corresponds to a thin layer: $d_{1n} = d_1/\lambda_t = 0.1$, where λ_t is the wavelength corresponding to the tuned frequency ω_t. In this case there is nearly no absorption up to $\Omega = 1$ while with a normalized thickness $d_{1n} = 0.4$ the absorption is brought down to $\Omega = 0.2$. Also, for frequencies such that $1 < \Omega < 10$ the absorption could vary by factors of $\pm 20\%$ in comparison to that of the semi-infinite layer.

Fig. 10a shows the absorption coefficient curves for a layer with normalized thickness $d_{1n} = 0.1$ and variable normalized cavity depth $d_{2n} = d_2/\lambda_t = 0.05, 0.1, 0.2$. Fig. 10b shows similar plots but this time with a fixed cavity depth $d_{2n} = 0.1$ and a variable layer of normalized thickness $d_{1n} = d_1/\lambda_t = 0.05, 0.1, 0.2$. As seen for the rigidly backed case the absorption coefficient is characterized by an oscillatory variation with frequency. The nature of this phenomenon is similar to that described above for the rigidly backed system except that in this case the indirect reflections are controlled by the waves propagating in the two layers (porous layer and air gap). As the air gap is increased the frequency amplitude of the first oscillation of the absorption curve is widened so that the absorption effect is extended to lower frequencies. Considering the absorption coefficient for the other case where the air gap is kept constant but the thickness of the layer is increased, which is shown in Fig. 10b, the oscillation effect in the absorption curve is smoothened over frequency.

Fig. 11a shows absorption curves for a rigidly backed layer with normalized thickness $d_{1n} = d_1/\lambda_t = 0.2$ and three different values of M (1, 3, 5) where λ_t is the wavelength corresponding to

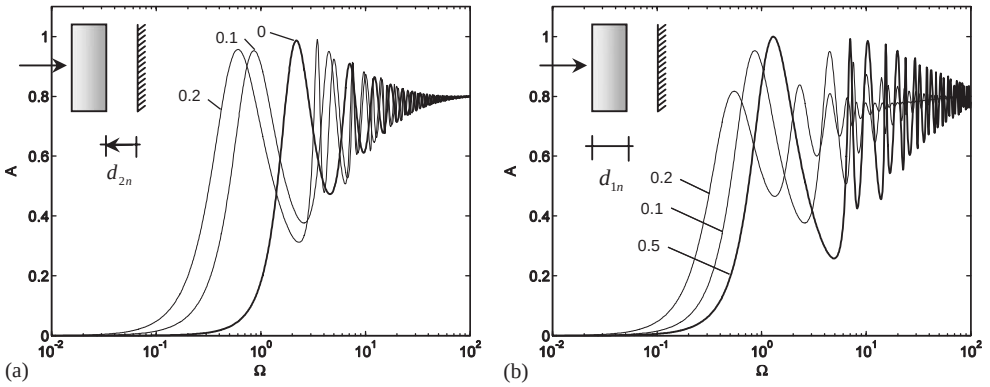

Fig. 10. Absorption coefficient curve for the air gap case. (a) The solid line corresponds to the limit case of cavity depth d_{2n} reducing to 0 (rigid backing case). The curves are plotted for a value of $M = 5$. $d_{1n} = 0.1$, $d_{2n} = 0$, 0.1, 0.2. (b) The curves are plotted for a value of $M = 5$ and $d_{1n} = 0.05$ (solid line), 0.1 and 0.2; $d_{2n} = 0.1$.

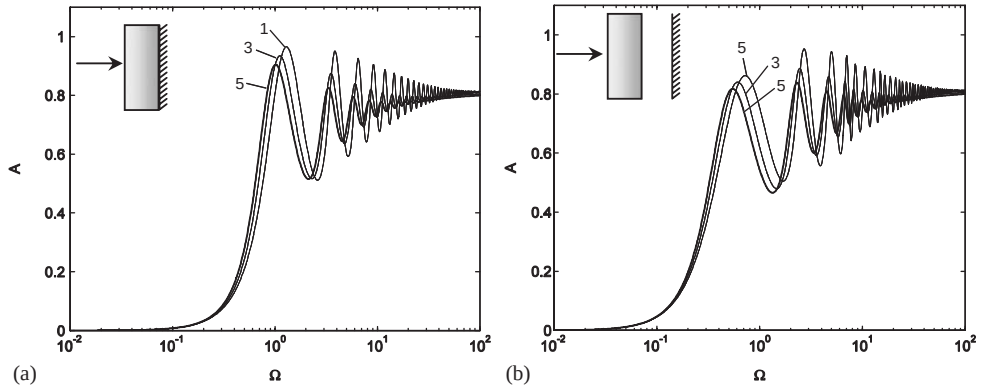

Fig. 11. (a) Absorption coefficient curves for rigid backing case and increasing values of M (1; 3; 5, respectively) and for $d_{1n} = d/\lambda_t = 0.2$. The thick line corresponds to $M = 5$. (b) Absorption coefficient curves for the air gap case and increasing values of M (1; 3; 5 respectively) and for $d_{1n} = d/\lambda_t = 0.2$ $d_{2n} = d_2/\lambda_t = 0.1$. The thick line corresponds to $M = 5$.

the tuned frequency ω_t. A different value of M indicates different properties of the material, and from the curves shown in the figure, it is clear that the knowledge of M can be helpful at the design stage of the material. In detail, a high value for M means less absorption coefficient oscillations in the high-frequency region, according to the higher values of damping represented by the imaginary part of the complex density as highlighted in Fig. 2. Fig. 11b shows similar plots but for the air gap case. In detail the cavity depth is $d_{2n} = 0.1$ and the thickness of the layer $d_{1n} = 0.2$. The effect is similar to that found for the rigidly backed configuration with a reduction of the oscillatory effect of the absorption at the higher frequencies.

The effect of the different volume of pores on the complex impedance has been presented in Section 2. Fig. 12 shows the corresponding curves of absorption coefficient for $h = 0.4$, 0.7 and 1 (solid curve for $h = 1$) for a rigidly backed layer of non-dimensional thickness $d_{1n} = 0.1$. It can be seen that reducing the porosity generates greater oscillations and smaller absorption, as the impedance of the surface becomes bigger.

5. Conclusions

The study presented in this paper is concerned with the acoustic properties of rigid-frame porous materials. Starting from the representation of the acoustic behaviour in terms of lumped parameter concepts (equivalent acoustic mass, stiffness and damping), a macroscopic wave model is presented which gives insight to the propagation, reflection and dissipation phenomena within a porous layer. This model has been experimentally validated by measuring absorption coefficients of a rubber granulate consolidated material with an impedance tube. Furthermore the effects of non-dimensional shape factor and porosity on absorption coefficients have been studied with the aim of connecting the geometrical and physical properties with the acoustic behaviour of rigid-frame porous materials.

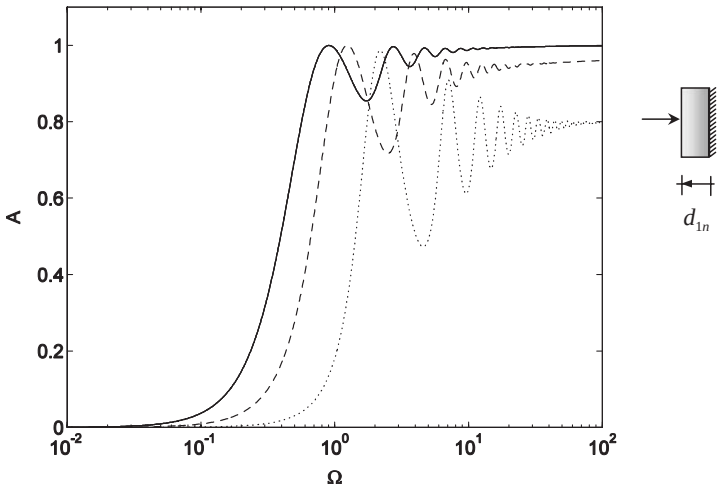

Fig. 12. Absorption coefficient curves for porosity $h = 0.4$ (dotted line) $h = 0.7$ (dashed line) and $h = 1$ (solid line). $M = 5$ and $d_{1n} = 0.1$. Rigid backing case.

Acknowledgements

The authors are grateful to M. Swift and K. Horoshenkov from the University of Bradford for providing samples of consolidated rubber granulate of tested tortuosity and porosity and to Y. Cho from the ISVR for his invaluable help with the measurements.

The work carried out by Silvia Rossetti was supported by the European Community with a Marie Curie Fellowship.

References

[1] J.F. Allard, *Propagation of Sound in Porous Media*, Elsevier Applied Science, London, 1993.
[2] D.L. Johnson, J. Koplik, R. Dashen, Theory of dynamic compressibility and tortuosity in fluid-saturated porous media, *Journal of Fluid Mechanics* 76 (1987) 379–402.
[3] D. Lafarge, P. Lemarinier, J.F. Allard, Dynamic compressibility of air in porous structures at audible frequencies, *Journal of the Acoustical Society of America* 102 (1997) 1995–2006.
[4] O. Umnova, K. Attenborough, K.M. Li, Cell model calculation of dynamic drag parameters in packings of spheres, *Journal of the Acoustical Society of America* 107 (2000) 3113–3119.
[5] M.J. Brennan, W.M. To, Acoustic properties of rigid frame porous materials—an engineering perspective, *Applied Acoustics* 62 (2001) 793–811.
[6] M. Swift, Physical Properties of Porous Recycled Materials. Ph.D. Thesis, University of Bradford, 2000.
[7] F. Fahy, *Foundations of Engineering Acoustics*, Academic Press, London, 2001.
[8] L.E. Kinsler, A.R. Frey, A.B. Coppens, J.V. Sanders, *Fundamentals of Acoustics*, fourth ed, Wiley, New York, 2000.
[9] J.F. Allard, M. Henry, J. Tizianel, L. Kelders, W. Lauriks, Sound propagation in air saturated random packing of beads, *Journal of the Acoustical Society of America* 104 (1998) 2004–2007.
[10] J. Tizianel, J.F. Allard, B. Castagnede, C. Ayrault, M. Henry, A. Gedeon, Transport parameters and sound propagation in air-saturated sand, *Journal of Applied Physics* 86 (1999) 5829–5834.

[11] M. Henry, P. Lemarinier, J.F. Allard, J.L. Bonardet, A. Gedeon, Evaluation of the characteristic dimensions for porous sound-absorbing materials, *Journal of Applied Physics* 77 (1995) 17–20.
[12] L. Cremer, M. Heckl, *Structure-Borne Sound*, second ed, Springer, Berlin, 1988.
[13] B.H. Song, J.S. Bolton, A transfer-matrix approach for estimating the characteristic impedance and wave numbers of limp and rigid porous materials, *Journal of the Acoustical Society of America* 107 (2000) 1131–1152.
[14] S. Rossetti, P. Gardonio, M.J. Brennan, Rigid frame porous materials: fundamental theory and applications, ISVR Technical Memorandum No. 911, University of Southampton, 2003.
[15] Y. Cho, P.A. Nelson, Least squares estimation of acoustic reflection coefficient, *Conference Proceedings, IOA Spring Conference*, 2002.